Prepared for submission to JCAP

Observable induced gravitational waves from an early matter phase

Laila Alabidi[a] **Kazunori Kohri**[b,c] **Misao Sasaki**[a] **Yuuiti Sendouda**[d]

[a]Yukawa Institute for Theoretical Physics, Kyoto University, Kyoto 606-8502, Japan
[b]Cosmophysics Group, Theory Center, IPNS, KEK, Tsukuba 305-0801, Japan
[c]The Graduate University for Advanced Study (Sokendai), Tsukuba 305-0801, Japan
[d]Graduate School of Science and Technology, Hirosaki University, Hirosaki, Aomori 036-8561, Japan

E-mail: laila@yukawa.kyoto-u.ac.jp, kohri@post.kek.jp,
misao@yukawa.kyoto-u.ac.jp, sendouda@cc.hirosaki-u.ac.jp

Abstract. Assuming that inflation is succeeded by a phase of matter domination, which corresponds to a low temperature of reheating $T_r < 10^9$GeV, we evaluate the spectra of gravitational waves induced in the post-inflationary universe. We work with models of hilltop-inflation with an enhanced primordial scalar spectrum on small scales, which can potentially lead to the formation of primordial black holes. We find that a lower reheat temperature leads to the production of gravitational waves with energy densities within the ranges of both space and earth based gravitational wave detectors.

Keywords: Inflation, Primordial Black Holes, Induced Gravitational Waves, DECIGO, BBO, LISA, KAGRA, LIGO

arXiv:1303.4519v2 [astro-ph.CO] 21 Mar 2013

Contents

1 Introduction **1**

2 Inflationary Parameters **2**

3 The temperature of reheating **3**

4 The spectrum of primordial black holes **4**
4.1 $M_{\rm BH}(T)$ and $k(M_{\rm BH})$ 4
4.2 T_r sets a cut-off 4

5 The spectra of induced gravitational waves **5**
5.1 Analytical Estimate for a Flat Spectrum 6
5.2 The evolution of the tensor mode 7
5.2.1 The accuracy of the sudden transition approximation 7
5.3 Transfer Function 9
5.4 Full numeric results for a flat spectrum 10

6 The Models of Inflation **13**
6.1 The Hilltop type model 13
6.2 The Running Mass Model 13

7 Results **14**

8 Discussion **20**

A The time integral during the radiation era **20**

1 Introduction

Induced gravitational waves are produced as a result of the interaction between scalar perturbations at second order in the post-inflationary universe. The amplitude of their spectra is dependent on the square of the primordial scalar spectrum [1–5], and a relatively large induced gravitational wave spectrum is expected from the generation of Primordial Black Holes (PBHs) [6–9]. In a previous paper Ref. [10] we evaluated the spectra of induced gravitational waves generated during a radiation dominated era from the hilltop-type and running mass models, which have been shown to be the only models which can lead to Primordial Black Holes [11, 12]. We showed that these models lead to an induced gravitational wave signature within the sensitivity ranges of planned gravitational wave detectors DECIGO and BBO [13–15]. We also found that the running mass model predicted spectra within the sensitivity of eLISA [16, 17]under the proviso that inflation is terminated early, with the intriguing factor that if we could motivate $N \ll 40$ we would get a detectable signature of PBHs with a mass compatible with Dark Matter.

In this paper, we assume that the universe undergoes a phase of early matter domination [18–21] [1], which lowers the reheat temperature as well as the number of allowed $e-$folds of inflation. The source term during the matter phase is constant, and as a result of the absence of pressure, the density contrast grows. This may result in perturbations entering the non-linear regime and decoupling from the Hubble flow. In our analysis we only assume a linear evolution of perturbations, and we account for the non-linear evolution by cutting off our analysis at some critical scale. To calculate this critical scale we begin by stating that perturbations in the early matter phase evolve as

---

[1] other scenarios are also possible [18, 19, 22, 23]

$$\frac{\delta\rho_m}{\rho} = \frac{2}{3\mathcal{H}^2}\nabla^2\Phi \tag{1.1}$$

where ρ_m is the energy density of matter, $\mathcal{H}$ is the conformal Hubble parameter and Φ is the gravitational potential. The evolution of the perturbations is therefore linear until the density contrast becomes of order unity which occurs at the scale [24]:

$$k_{NL} \sim \mathcal{P}_\zeta^{-1/4} k_r \tag{1.2}$$

where k_r is the scale which re-enters the horizon at the time of reheating, $\mathcal{P}_\zeta$ is the primordial spectrum and k_{NL} is the critical scale at which we terminate our calculation.

This paper is organised as follows, in section 2 we review the parameters of inflation, in section 3 we present the thermal history of the universe, relating the temperature of reheating to the relevant scale of reheating, in section 4 we caclulate the bounds on the primordial spectrum from PBHs, in section 5 we review the spectrum of induced gravitational waves produced during the early matter phase, in section 6 we review the models of inflation that can lead to a detectable limit of induced gravitational waves and penultimately in section 7 we present the results with the final discussion presented in section 8.

The following conventions are utilised in this paper: τ refers to conformal time and is related to proper time t as $d\tau = dt/a$, a is the scale factor, and the conformal Hubble parameter $\mathcal{H}$ is related to the Hubble parameter $H \equiv \dot{a}/a$ as $\mathcal{H} = aH$. Scales are denoted by k, are given in units of inverse megaparsec Mpc^{-1} and are related to physical frequency f as $f = ck/(2a\pi)$ where c is the speed of light. We assume a radiation dominated universe at the time of the formation of the gravitational waves, in which case we have $a = a_0(\tau/\tau_0)$, $\mathcal{H} = \tau^{-1}$, and the scale at re-entry is $k = \tau^{-1}$.

2 Inflationary Parameters

Models of inflation can be parametrised by the slow roll parameters [25] :

$$\begin{aligned}\epsilon &= \frac{m_{\mathrm{Pl}}^2}{2}\left(\frac{V_{,\varphi}}{V}\right)^2 \\ \eta &= m_{\mathrm{Pl}}^2 \frac{V_{,\varphi\varphi}}{V} \\ \xi^2 &= m_{\mathrm{Pl}}^4 \frac{V_{,\varphi}V_{,\varphi\varphi\varphi}}{V^2}\end{aligned} \tag{2.1}$$

where V is the potential, and derivatives are with respect to the inflaton field φ. These are related to the observational parameters, the spectral index n_s, the running of the spectral index n_s' and the scalar spectrum $\mathcal{P}_\zeta$ as:

$$
\begin{aligned}
n_s &= 1+2\eta-6\epsilon \\
n_s' &= 16\epsilon\eta-24\epsilon^2-2\xi^2 \\
\mathcal{P}_\zeta &= \frac{1}{24\pi^2 m_{\rm Pl}^4}\frac{V}{\epsilon}
\end{aligned}
\tag{2.2}
$$

We use a time re-parametrisation, $N=\ln\left(\frac{a_e}{a_*}\right)$, where the subscripts e and $*$ denote the end of inflation and the time of horizon exit respectively. This is related to the potential in the slow roll limit as:

$$
N \simeq m_{\rm Pl}^{-2}\int_{\varphi_e}^{\varphi_*}\frac{V}{V'}d\varphi \tag{2.3}
$$

and to the scale at horizon exit as [25]:

$$
N(k_0)-N(k)=\ln\left(\frac{0.002}{k}\right). \tag{2.4}
$$

where $k_0 = 0.002\text{Mpc}^{-1}$ is the pivot scale, and in this paper we effectively take $N(k_0)=0$.

We use the latest data release from the WMAP mission [26, 27], for the WMAP data combined with BAO and H0 data with a null tensor prior. Throughout this paper we take $n_s = 0.96$ and $n_s' \leq 0.0062$.

3 The temperature of reheating

The number of $e-$folds can be related to the temperature of reheating T_r as [28, 29]

$$
N = 56-\frac{2}{3}\ln\left(\frac{10^9\text{GeV}}{T_r}\right) \tag{3.1}
$$

where we have taken the energy scale of inflation to be the SUSY GUT scale $\sim 10^{16}$GeV. Assuming SUSY means that $N_{max}=56$, otherwise we can push this estimate up to $N_{max}\sim 60$. In this work we are only interested in reducing the number of $e-$folds via the inclusion of an early matter phase. The thermal history of the universe can support a reheat temperature down to 1MeV, as this is the temperature below which Neutrinos fail to thermalise and affect big-bang nucleosynthesis[30–33] and hence $N \gtrsim 37$. To relate T_r to the scale k_r we assume the conservation of entropy which gives

$$
\begin{aligned}
H &= g_{*s}(T_r)^{1/2}\frac{T_r^2}{M_G} \\
\frac{a}{a_0} &= \frac{T_0}{T_r}[g_{*s}(T_0)/g_{*s}(T_r)]^{1/3}
\end{aligned}
\tag{3.2}
$$

where g_{*s} is the number of degrees of freedom, M_G is the gravitational scale ($M_G = M_p/\sqrt{8\pi} \simeq 2.4\times10^{18}$GeV) and since $k=aH/a_0$ we get the scale which re-enters the horizon at the end of reheating k_r:

$$
k_r \sim 1.7\times10^{16}\text{Mpc}^{-1}\left(\frac{\rm T_r}{10^9\text{GeV}}\right)\left(\frac{\rm g_{*s}}{106.75}\right)^{1/6} \tag{3.3}
$$

4 The spectrum of primordial black holes

If the primordial spectrum of perturbations towards the end of inflation is large enough, i.e if the density contrast exceeds $\delta \approx 1/3$, perturbations can collapse to form primordial black holes. Based on this, constraints can be placed on the spectrum based on astrophysical phenomena [34, 35]. In our previous paper, we numerically converted the mass fraction of the PBHs into a power spectrum. To perform this analysis we assumed a gaussian distributed energy perturbation [2] and a very large reheat temperature $T_r \gg 10^{10}$GeV. In this paper, we update this calculation for lower reheat temperatures.

4.1 $M_{\rm BH}(T)$ and $k(M_{\rm BH})$

The comoving wavenumber corresponding to the Hubble radius at temperature T is

$$k = \frac{a\,H}{c} \approx 1.71 \times 10^{16}\,\mathrm{Mpc}^{-1} \left(\frac{g_{*s}}{106.75}\right)^{1/6} \left(\frac{T}{10^9\,\mathrm{GeV}/k_{\rm B}}\right) . \tag{4.1}$$

On the other hand, the mass of PBHs produced at temperature T is

$$\begin{aligned} M_{\rm BH} &= \gamma\,\frac{4\pi}{3}\,\frac{\rho}{H^3} = \frac{3\sqrt{5}}{4\pi^{3/2}\,G^{3/2}}\,\gamma\,g_{*s}^{-1/2}\,T^{-2} \\ &\approx 0.916\,\times 10^{-20}\,M_\odot \left(\frac{\gamma}{(1/\sqrt{3})^3}\right) \left(\frac{g_{*s}}{106.75}\right)^{-1/2} \left(\frac{T}{10^9\,\mathrm{GeV}}\right)^{-2} , \end{aligned} \tag{4.2}$$

where γ is a numerical factor and $M_\odot = 1.989 \times 10^{33}\,$g. Eliminating T, we find

$$\begin{aligned} k &= \frac{\pi^{3/4}\,g_{*s0}^{1/3}\,T_{\gamma 0}}{45^{1/4}\,G^{1/4}}\,\frac{g_{*s}^{1/4}}{g_{*s}^{1/3}\,\sqrt{M_{\rm BH}/\gamma}} \\ &\approx 1.71 \times 10^{16}\,\mathrm{Mpc}^{-1} \left(\frac{g_{*s}}{106.75}\right)^{-1/12} \left(\frac{\gamma}{(1/\sqrt{3})^3}\right)^{1/2} \left(\frac{M_{\rm BH}}{0.916 \times 10^{-20}\,M_\odot}\right)^{-1/2} . \end{aligned} \tag{4.3}$$

In our numerical calculation we adopt $\gamma = 1$ and $g_{*s} = 106.75$ for whatever values of T, which implies

$$M_{\rm BH} \approx 0.946 \times 10^{28}\,\mathrm{g} \left(\frac{T}{10^2\,\mathrm{GeV}}\right)^{-2} , \quad k \approx 1.67 \times 10^{9}\,\mathrm{Mpc}^{-1} \left(\frac{M_{\rm BH}}{10^{28}\,\mathrm{g}}\right)^{-1/2} . \tag{4.4}$$

These are only precise for $M_{\rm BH} \lesssim 10^{28}\,$g but the error will not be very large even for larger PBHs.

4.2 T_r sets a cut-off

Our setup is such that the universe after inflation is once dominated by an oscillating scalar field and then reheated to the temperature T_r. We neglect any PBHs produced before reheating (i.e., during the early matter domination) and even those produced after reheating if it happens on sub-horizon scales. This gives us conservative PBH constraints. In Ref. [43], the authors discussed PBH formation in matter-dominant universe. Assuming a spherical collapse of a dense region into a PBH, they obtain the result that more PBHs tend to be

---

[2] see Ref. [36–42] for alternative scenarios

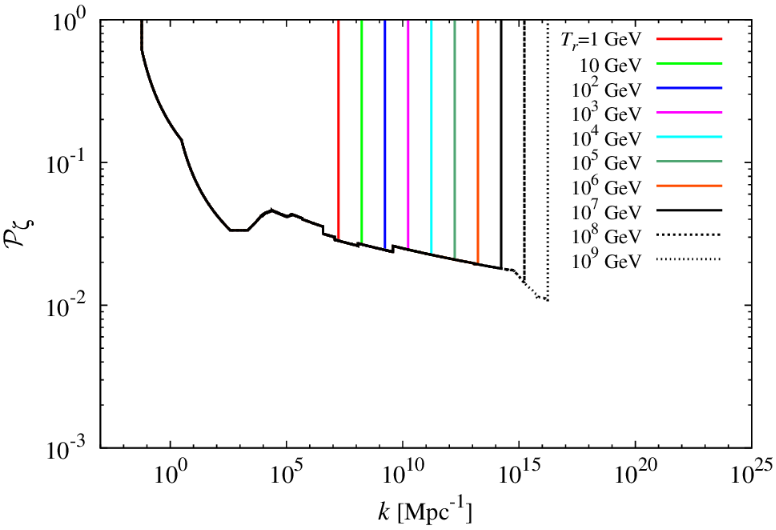

Figure 1. The PBH bound on the primordial spectrum for various cut-off masses, as defined in the figure legend.

produced. This would be reasonable since the pressure $P = 0$. However, they did not consider any non spherical effects, which cause the non-spherical morphologies to evolve during the collapsing phase, which would have prevented a further collapse. To get a rigorous bound on the PBH spectrum for the early matter phase, we need numerical simulations to obtain the correct criterion for matter collapse in matter domination analogous to the radiation domination case that $1/3 < \delta < 1$ for matter to collapse into a PBH.

In fact, in this treatment there arises a cut-off PBH mass determined by the reheat temperature:

$$M_{\rm BH,co} \approx 0.946 \times 10^{32}\,{\rm g} \left(\frac{T_r}{1\,{\rm GeV}}\right)^{-2}, \tag{4.5}$$

which corresponds to a cut-off wavenumber

$$k_{\rm co} \approx 1.71 \times 10^7\,{\rm Mpc}^{-1} \left(\frac{T_r}{1\,{\rm GeV}}\right). \tag{4.6}$$

The scalar perturbations with $k > k_{\rm co}(T_r)$ may not constrained by PBHs, see Fig. 1.

5 The spectra of induced gravitational waves

We follow the analysis of Ref. [4] with much of the notation of Ref. [5]. The spectrum of induced gravitational waves generated during an early matter phase was first calculated in Ref. [24] and is given as

$$\mathcal{P}_h(k) = \frac{2}{x^3}\left(\frac{40}{3}\right)^2 \int_0^\infty dv \int_{|v-1|}^{|v+1|} dy \frac{v^2}{y^2}(1-\mu^2)^2 \mathcal{P}_\zeta(ky)\mathcal{P}_\zeta(kv) I^2_{MDS} \tag{5.1}$$

where $x = k\tau$, k is the scale, τ is conformal time, $v = \tilde{k}/k$ the ratio of the incoming to outgoing scales, $y = \sqrt{1 + v^2 - 2v\mu}$, μ is the cosine of the angle between the incoming and outgoing scales, $\mathcal{P}_\zeta$ is the spectrum of primordial fluctuations, in this case generated during inflation, and I_{MDS} is the time integral given as

$$I_{MDS} = \frac{3x\cos(x) - 3\sin(x) + x^3}{x^{3/2}} \, . \tag{5.2}$$

We have taken the lower limit to be $x = 0$, and terminated the integration at $x = k\tau_r$, where τ_r is the conformal time at the end of the reheating era.

The spectrum for induced gravitational waves during radiation domination is given by [4, 5]

$$\mathcal{P}_h(k) = \frac{k^2}{x^2}\int_0^\infty dv \int_{|v-1|}^{|v+1|} dy \frac{v^2}{y^2}(1-\mu^2)^2\mathcal{P}_\zeta(kv)\mathcal{P}_\zeta(ky)\tilde{I}_1\tilde{I}_2. \tag{5.3}$$

where the time integrals, $\tilde{I}_1$ and $\tilde{I}_2$, used in this paper are derived in [10] and given in appendix A.

5.1 Analytical Estimate for a Flat Spectrum

In this section we assume a flat spectrum and set $\mathcal{P}_\zeta(k) = \Delta_R \simeq 10^{-9}$. Then the spectrum can be written as:

$$\mathcal{P}_h(k) = 2\left(\frac{40}{3}\right)^2 \Delta_R^2 \int dv \int dy (1-\mu^2)^2 \left(\frac{v}{y}\right)^2 \frac{I_{MD}^2}{x^3} \tag{5.4}$$

consider the term $I_{MDS}/x^{3/2}$:

$$\frac{I_{MD}}{x^{3/2}} = \left[1 + \frac{3}{x^3}\left(x\cos(x) - \sin(x)\right)\right] \equiv I_{MDS} \tag{5.5}$$

and it is clear that for $x \gg 1$ I_{MDS} approaches a constant. Substituting this into our equation for the spectrum we have

$$\mathcal{P}_h(k) = 2\left(\frac{40}{3}\right)^2 \Delta_R^2 \int dv \int dy (1-\mu^2)^2 \left(\frac{v}{y}\right)^2 I_{MDS}^2 \tag{5.6}$$

recall that $x = k\tau$, where τ is the limit of our time integral which we take to be the end of the reheating phase $\tau_r = 2/k_r$. Therefore x_r is much greater than 1 for most of the scales we consider. Hence we can pull I_{MDS} out of the integral

$$\mathcal{P}_h(k) = 2\left(\frac{40}{3}\right)^2 \Delta_R^2 I_{MDS}^2 \int dv \int dy (1-\mu^2)^2 \left(\frac{v}{y}\right)^2 \tag{5.7}$$

and the integrals can be performed analytically. We find that the analytical equation is compatible with with numerical calculation for a flat spectrum.

For scales $k_r < k < k_{max}$ the spectrum is then

$$\frac{\mathcal{P}_h}{\Delta_R(k)^2} \approx 2\left(\frac{40}{3}\right)^2 \left(\frac{16\,k}{35\,\mathrm{k_{max}}} + \frac{16\,\mathrm{k_{max}}}{15\,k} - \frac{4\,\mathrm{k_r}^4}{15\,k^4} + \frac{8\,\mathrm{k_r}^6}{105\,k^6}\right) \tag{5.8}$$

where we have taken the upper limit on v, $v_{max} = k_{max}/k$ and the lower limit to be $v_{min} = k_{min}/k$, and we took $k_{min} = k_r$ where k_r is the scale that re-entered the horizon at the end of the matter era, we have also taken $I_{MDS} \approx 1$. By only considering scales which re-enter the horizon near $k \sim k_r$, those whose amplitudes have grown the most, Eq. (5.8) can be reduced to $\sim 356(16k_{max}/(15k))$ which for $k_{max} = k_{NL} \sim 141k_r$ and $k \sim k_r$ is 10^5. Taking instead $k_{max} = 10^3 k_r$ leads to a spectrum maximum of $\approx 10^6$ as is confirmed in the full numerical calculation shown in Fig. 4.

5.2 The evolution of the tensor mode

Defining $v_{\rm k} = ah_{\rm k}$, the equation of motion for the tensor modes is given as

$$v_{\rm k}'' + \left(k^2 - \frac{a''}{a}\right) = aS_{\rm k} \tag{5.9}$$

and can be solved approximately for the full evolution of the universe. Using step and boxcar functions, the source term $aS_{\rm k}$ can be written out as

$$a\mathcal{S}_{\rm k} \propto k^2\tau^2 \left(\theta(\tau_r - \tau) + \frac{\tau_r^4}{\tau^4}\Pi_{\tau_r\tau_{eq}} + \left(\frac{\tau_r}{\tau_{eq}}\right)^4 \theta(\tau - \tau_{eq})\right) \tag{5.10}$$

where we have taken $\mathcal{S} \propto \tau^{-3}$ during radiation domination, θ is the heaviside step function and $\Pi_{\tau_r\tau_{eq}} = \theta(\tau - \tau_r) - \theta(\tau - \tau_{eq})$ is the boxcar function. The scale factor can be written out in a similar fashion

$$a \propto \tau^2\theta(\tau_r - \tau) + \tau\tau_r\Pi_{\tau_r\tau_e} + \left(\frac{\tau_r}{\tau_{eq}}\right)\tau^2\theta(\tau - \tau_{eq}) \tag{5.11}$$

For sub horizon modes, $k \gg 1/\tau$, we obtain the solution plotted black in Fig. 2. In this scenario, inflation gives way to an early phase of matter domination which ends when $\tau = \tau_r$ and is followed by a phase of radiation domination that is overtaken by matter at $\tau = \tau_{eq}$. The source term is at first constant, then when $\tau_r < \tau < \tau_{eq}$ it decays at a rate $\propto \tau^{-3}$ and constant again for $\tau > \tau_{eq}$. The amplitude of the sub-horizon tensor modes which re-enter the horizon during early matter domination is held at a constant until τ_r, when begins to freely propagate and decay at a rate $\propto a^{-1}$, until it becomes equal to the source term and held at a constant value. The superhorizon modes grow until $\tau = \tau_r$, are held at a constant between $\tau_r < \tau < \tau_{eq}$ and grow again for $\tau > \tau_{eq}$.

5.2.1 The accuracy of the sudden transition approximation

Throughout this paper we have utilised the sudden transition approximation between an early matter phase and radiation. In this section we investigate the effect a smoother turnover has on the tensor modes generated during the early matter phase. For this we make the following approximations for the scale factor and source term

$$\begin{aligned} a &= 2a_r\left(\frac{\tau}{\tau_r}\right)^2 \frac{1}{(1 + (\tau/\tau_r)^n)^{1/n}} \\ S &= \frac{k^2}{1 + (\tau/\tau_r)^4} \end{aligned} \tag{5.12}$$

where n is an integer. We plot the results for $n = 1$, $n = 8$ and the sudden transition approximation in Fig. 3. As is clear from the figure, in all cases the tensor modes approach the freely oscillating stage during radiation domination, however, the smooth turnover results in a smaller amplitude of an order of magnitude. We also note that $n = 8$ is very close to the sudden transition approximation, and that $n = 1$ is less than an order of magnitude smaller that it. This phenomenon requires further investigation.

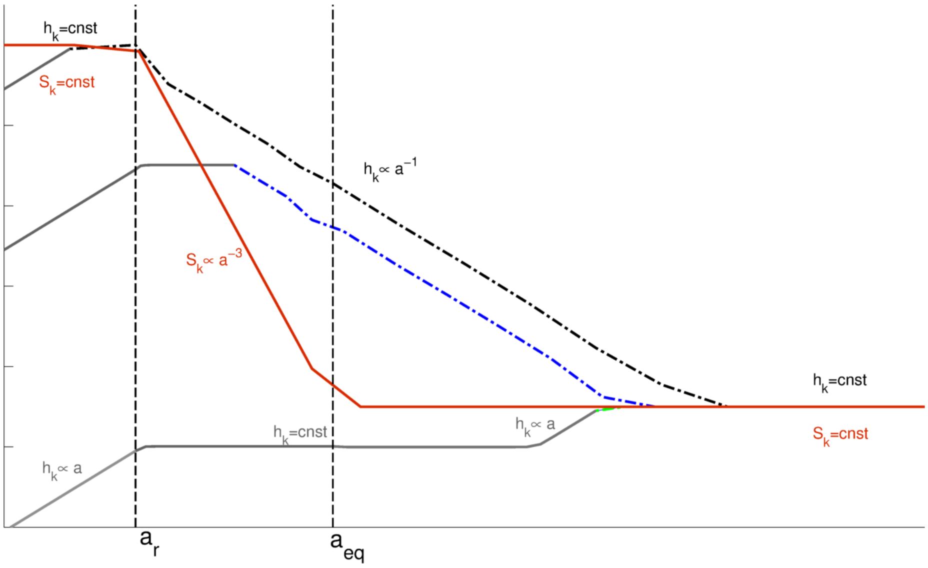

Figure 2. A schematic of the evolution of tensor modes on different scales with respect to the logarithm of the scale factor. The solid red line depicts the evolution of the source term between epochs. a_r is the scale factor at reheating and a_{eq} is the scale factor at radiation-matter equality. Grey lines represent super-horizon modes. The black dash-dot line represents the evolution of a mode which enters during EMD. The blue dash-dot line represents the amplitude of the mode which enters during RD and the green line, which is barely visible at the right hand side of the plot, represents the mode which enters during the current epoch (assuming no acceleration).

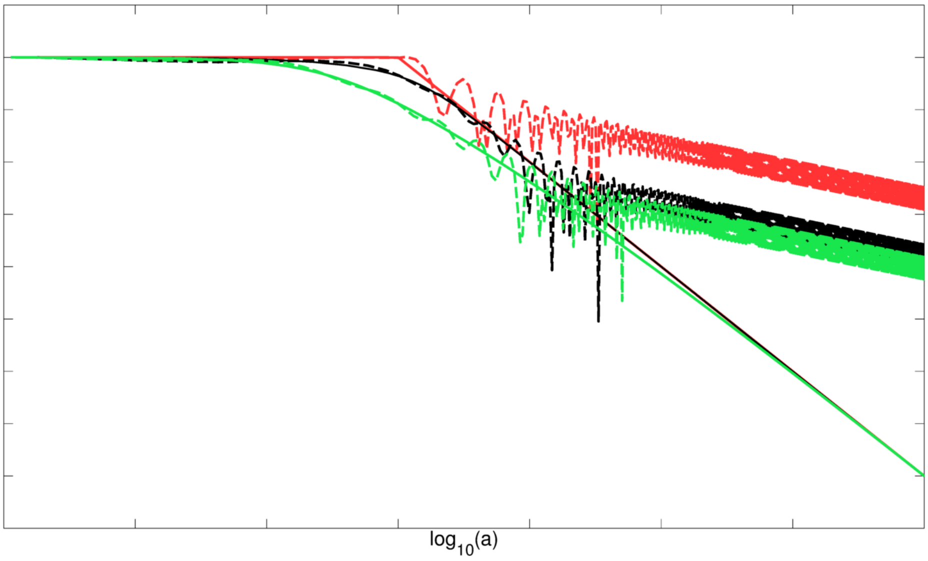

Figure 3. The solid lines represent the source term, the red is the sudden transition approximation Eq. (5.10), the green is the smooth turnover with $n = 1$, and the black is $n = 4$. The dashed lines represent the tensor modes. As we can see the tensor modes do approach the freely oscillating limit, but there is some loss of amplitude with respect to the sudden transition approximation

5.3 Transfer Function

Detectors of gravitational waves will place a bound on the energy density of gravitational waves, defined as [44]:

$$\Omega_{\rm GW}(f) = \frac{1}{\rho_c}\frac{d\rho_{\rm GW}}{d\ln f} \tag{5.13}$$

where f is the frequency, ρ_c is the critical energy density defining the coasting solution of the Friedman equation and $\rho_{\rm GW}$ is the energy density of gravitational waves. This is related to the primordial spectrum via a transfer function, $\Omega = t^2(k,\tau)\mathcal{P}_h(k)$. Scales that re-enter the horizon during a period of early matter domination experience a constant source term, and the amplitude of the tensor mode is kept at it's super horizon value. However once the universe enters the radiation epoch the source term decays as does the amplitude of the tensor modes, as is depicted in Fig. 2.

In Ref. [5] they show that for scales smaller than some critical scale, which our scales of interest are, the transfer function is

$$t(k,\tau) = \frac{a_k}{a(\tau)} \tag{5.14}$$

where a_k is the scale factor when the scale k enters the horizon. To be precise, it is the scale factor at the time when the source term at that scale begins to decay. That is, for scales that enter the horizon during early matter domination, $a_k = a_r$. Our transfer function is then

$$\begin{aligned} t(k,\tau) &= \frac{a_r}{a(\tau)} \\ &= \frac{a_r}{a_{eq}}\frac{a_{eq}}{a(\tau)} \\ &= \frac{a_{eq}}{a_r}\frac{k_{eq}}{k_r} \end{aligned} \tag{5.15}$$

where subscript eq is that of radiation-matter equality and the relative energy of scalar-induced gravitational waves is

$$\begin{aligned} \Omega_{GW}(k,\tau) &= \frac{a(\tau)k^2}{a_{eq}k_{eq}^2}t^2(k,\tau)\mathcal{P}_h \\ &= \frac{1}{(1+z_{eq})}\left(\frac{k}{k_r}\right)^2\mathcal{P}_h \end{aligned} \tag{5.16}$$

where z is the redshift. For scales which re-enter the horizon during radiation domination, the relative energy of induced gravitational waves is

$$\Omega_{GW} = \frac{1}{1+z_{eq}}\mathcal{P}_h(k)\ . \tag{5.17}$$

5.4 Full numeric results for a flat spectrum

To get the full spectrum of induced gravitational waves for an early matter phase followed by a radiation phase we evaluate

$$\begin{aligned}
\mathcal{P}_h(k) &= \left(\int_0^{x_r} F(v,y,\tau_1)d\tau_1 + \int_{x_r}^{x} F(v,y,\tau_2)d\tau_2\right) \\
&= \int_0^{x_r} F(v,y,\tau_1)F(v,y,\tau_2)d\tau_1 d\tau_2 + \\
&\quad \left(\int_0^{x_r} F(v,y,\tau_1)d\tau_1 \int_{x_r}^{x} F(v,y,\tau_2)d\tau_2 + \int_0^{x_r} F(v,y,\tau_2)d\tau_2 \int_{x_r}^{x} F(v,y,\tau_1)d\tau_1\right) \\
&\quad + \int_{x_r}^{x} F(v,y,\tau_2)F(v,y,\tau_1)d\tau_1 d\tau_2 \\
&= \mathcal{P}_{h,matter} + C_{h,cross} + \mathcal{P}_{h,radiation} \\
&\approx \mathcal{P}_{h,matter} + \mathcal{P}_{h,radiation}
\end{aligned} \tag{5.18}$$

where $F(v,y,\tau)$ is the integral over v,y in Eq. (5.3), and we drop the cross terms arising from $< \Phi_{matter}\Phi_{radiation} >$ in the last line. This approximation is reasonable since the cross terms are only of significance at $k \sim k_r$.

Figure 4 is a depiction of the spectrum of induced gravitational waves arising from a flat primordial spectrum of density perturbations; $n_s = 1$. This figure was generated mainly for illustrative purposes, and as such we have chosen k_{NL} to be 10^3 times as large as the value calculated using Eq. (1.2). We assume that modes with $k > k_{NL}$ do not experience the constant source term. Scales which are still super-horizon at the end of the early-matter phase have a spectrum $\mathcal{P}_h \propto k^3$ and therefore become rapidly smaller than the spectrum generated by the pure radiation source term. That means that for modes which enter the horizon soon after τ_r we need only consider the convolution of modes with those that enter during the radiation era.

We present the results for a flat spectrum at various reheat temperatures in Fig. 5, where we have taken the limits on v to be $v_{min} = k_r/k$ and $v_{max} = k_{NL}/k$ with the latter upper bound accounting for the non-linear cutoff. We could have modified the calculation and checked for each v and y that $\tilde{k} < k_{NL}$ and $|\tilde{\mathbf{k}} - \mathbf{k}| < k_{NL}$, however simply modifying the limits of v has the same effect.

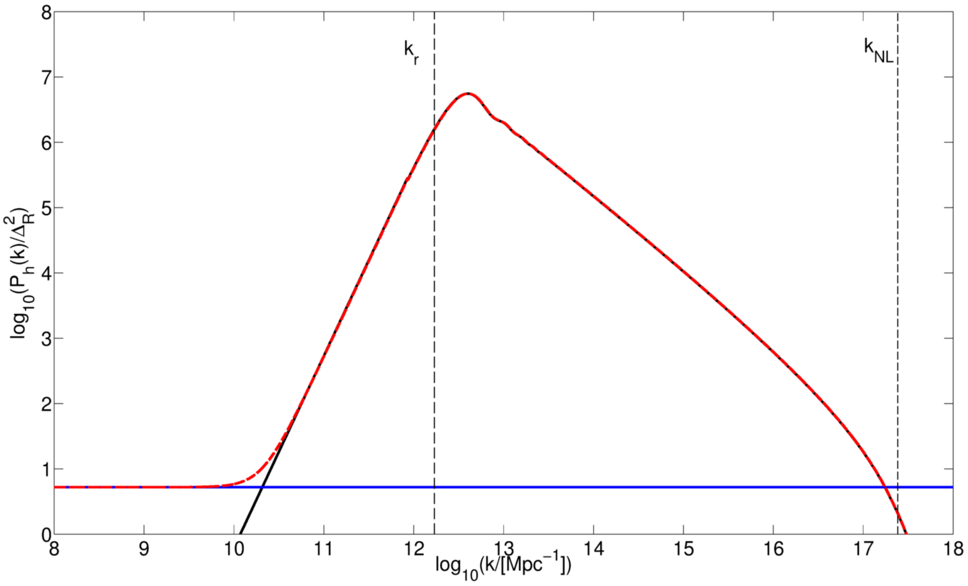

Figure 4. We plot the spectrum of induced gravitational waves for a flat primordial spectrum with $T_r = 10^9$GeV. The spectrum for scales that re-enter the horizon deep in the radiation era have a flat spectrum, due to the fact that the source term is a decaying function and thus the modes oscillate freely, and is represented by the solid blue line. The solid black line represents the modes that re-enter the horizon during the early matter phase ($k > k_R$). The The red dashed line is the complete spectrum, assuming an early matter phase followed by a phase of radiation domination. The spectrum for $k > k_{NL}$ behaves as $\mathcal{P}_h \propto 1/k^4$, as $\mathcal{P}_h \propto 1/k$ for $k_r < k < k_{NL}$, as $\mathcal{P}_h \propto k^3$ for $k \lesssim k_r$ and as $\mathcal{P}_h \sim$ constant for $k \ll k_r$. One can think of this as follows: modes that re-enter the horizon during the radiation phase but with $k \sim k_r$, i.e. near the EMD phase, will interact with modes that re-entered during EMD and hence their behaviour/characteristics are modified from the instant reheating scenario. We have utilised a simplified analysis, in that $\mathcal{P}_h(k) = \mathcal{P}_{h_{matter}}(k) + \mathcal{P}_{h_{rad}}(k)$.

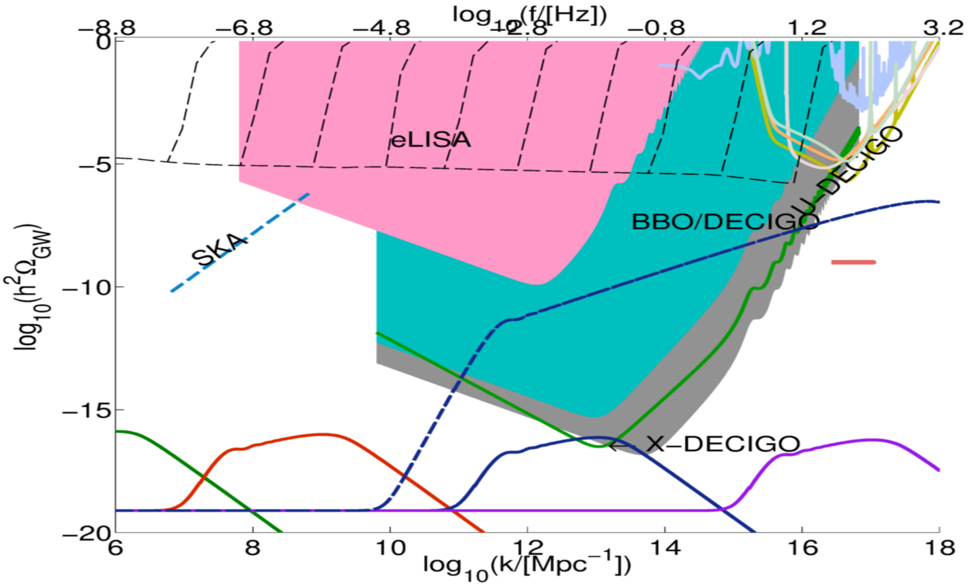

Figure 5. We plot the spectrum of induced gravitational waves for a flat primordial spectrum with various reheat temperatures and the cutoff scale $k_{max} = k_{NL}$. The black dashed lines correspond to the PBH bound assuming (from left pseudo-vertical line to right pseudo-vertical line) $T_r = 1\text{GeV}, 10\text{GeV}, 10^2\text{GeV}, 10^3\text{GeV}, 10^4\text{GeV}, 10^5\text{GeV}, 10^6\text{GeV}, 10^7\text{GeV}, 10^8\text{GeV}$ and 10^9GeV. The cluster of solid lines in the top right corner are the sensitivity ranges of ground based detectors, LIG0 S5 and S6 [45], and KAGRA [46], while the thick horizontal salmon pink line is the forecast sensitivity of Advanced LIGO [47, 48]. Also shown is the sensitivity limit of the Square Kilometre Array (SKA) [49–52]. The green, red, blue and purple solid lines correspond to taking $T_r = 1\text{MeV}$, 1GeV, 10^4GeV, and 10^8GeV. The blue dashed line is the spectrum for $T_r = 10^4\text{GeV}$ without terminating at k_{NL}. It is interesting to note that even a flat primordial spectrum can lead to a spectrum of induced gravitational waves detectable by cross-correlated DECIGO

6 The Models of Inflation

The spectrum of induced gravitational waves is directly proportional to the square of the primordial spectrum and is therefore clear that for an enhanced spectrum of induced gravitational waves one needs an enhanced primordial spectrum. Since at the pivot scale the spectrum is tightly constrained by CMB data we need to go beyond this and consider models which enhance the spectrum on small scales. Phenomenologically, the two models of inflation that exhibit this property [11, 12] are the running mass model and the hilltop model, depicted in Fig. 6.

6.1 The Hilltop type model

Identified in Ref. [11] as the phenomenological form necessary for PBH formation this model has the potential [53, 54]:

$$V = V_0\left(1 + \eta_p \varphi^p - \eta_q \varphi^q\right) \tag{6.1}$$

where the coupling terms η_p and η_q are less than 1 and $p < q$ to get the shape in Fig. 6. Certain realisations in super gravity can be found; see for example Refs. [11, 55–60].

This model is very compatible with WMAP data, and as such many of the model's terms are not ruled out, but in this analysis we add the extra requirement that the model is maximised at small scales and yet still remain within the PBH bound. We also take the basic number of $e-$folds to be $N = 56$. Parameter selection criteria is explained in more detail in Ref. [10].

6.2 The Running Mass Model

This model is the basic ϕ^2 model with a varying mass term that arises in taking renormalised group equations, and is given as [8, 61–68]

$$\frac{V}{V_0} = 1 - \frac{B_0}{2}\varphi^2 + \frac{A\varphi^2}{2(1+\alpha\ln(\varphi))^2}\ . \tag{6.2}$$

In this case we select parameters which satisfy $n_s = 0.96$, $n_s' = 0.0039$ and $n_s' = 0.0043$, which for $T_r > 10^9$GeV are terminated at $N =$ and $N =$ respectively.

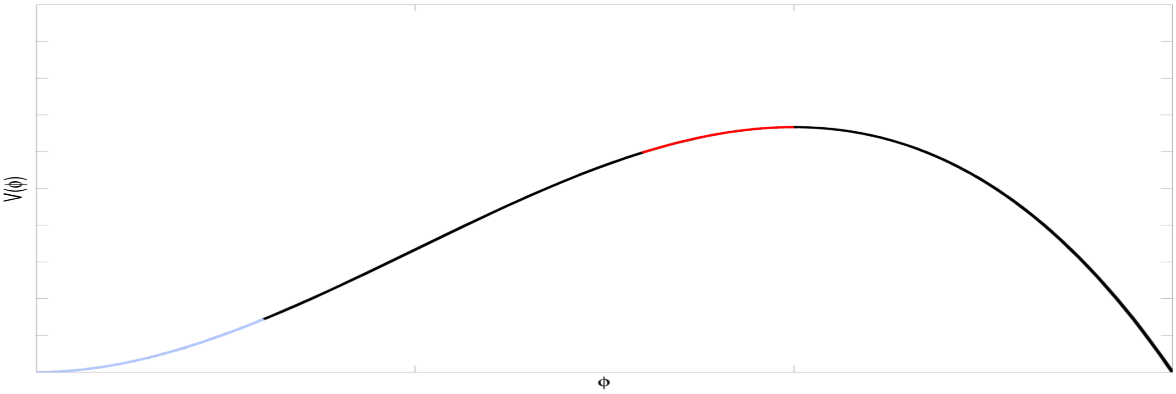

Figure 6. An illustration of the Hilltop-type and running models. In our scenario scales of cosmological interest during the hilltop regime (indicated with red), and the end of inflation occurs once the inflaton has reached a flatter region of the potential (indicated with blue).

7 Results

We plot results for the hilltop model for $p = 2$ and $q = 2.3, 3, 4$, and for the running mass models which satisfy $n_s = 0.96$ and $n_s' < 0.0062$ with $N \sim 57$. These are plotted in Figures. 7,8, 9, 10, 11 and 12 for a range of reheat temperatures $1\mathrm{GeV} < \mathrm{T_r} < 10^9\mathrm{GeV}$ [3]. Each reheat temperature modifies the maximum allowed number of $e-$folds N_{max} and therefore we have integrated only up to $k_{max} = k_{pivot}e^{N_{max}}$, except for in the case when $k_{max} > k_{NL}$ where we only integrate up to k_{NL}. In the final figure, Fig. 12 we have plotted the results of the hilltop and running mass models for a reheat temperature of $T_r = 10^6\mathrm{GeV}$.

In our previous paper Ref. [10], we calculated the spectrum of Induced Gravitational Waves for the running mass models with large running $0.0067 < n_s' < 0.012$ which is no longer supported by the latest WMAP release [26, 27]. On a related note, to motivate $N < 37$ by modifying the reheat temperature would require $T_r < 1\mathrm{MeV}$ which is unsupported by theory.

We also find that for the running mass model satisfying $N = 38$ $e-$folds, the corresponding induced gravitational waves spectra were not within the sensitivity ranges of any of the experiments. However, if the k_{NL} cutoff can be relaxed, the spectra may very well be within the ranges of SKA and PULSAR.

---

[3] There is an error in our previous paper, a missing factor of 4 in the f function which means that our previous results are 4^2 times smaller than they should be, this is corrected for here.

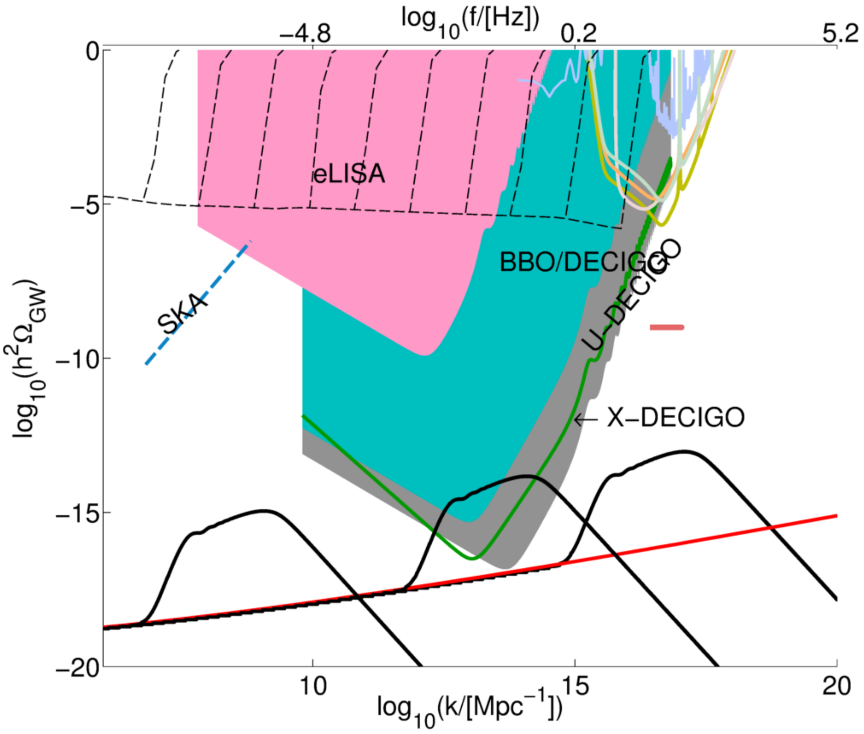

Figure 7. The spectra of induced gravitational waves for the Hilltop model with $p = 2$ and $q = 3$, with $k_{max} = k_{NL}$. The black dashed lines and the cluster of solid lines in the right hand corner are defined in Fig. 5. The red line represents the induced gravitational wave spectrum for $T_r \gg 10^{10}\mathrm{GeV}$ and $N = 55$ $e-$folds. From right to left the black solid lines correspond to the induced gravitational wave spectrum for reheat temperatures of $T_r = 10^8\mathrm{GeV}$, $T_r = 10^5\mathrm{GeV}$, and $T_r = 1\mathrm{GeV}$.

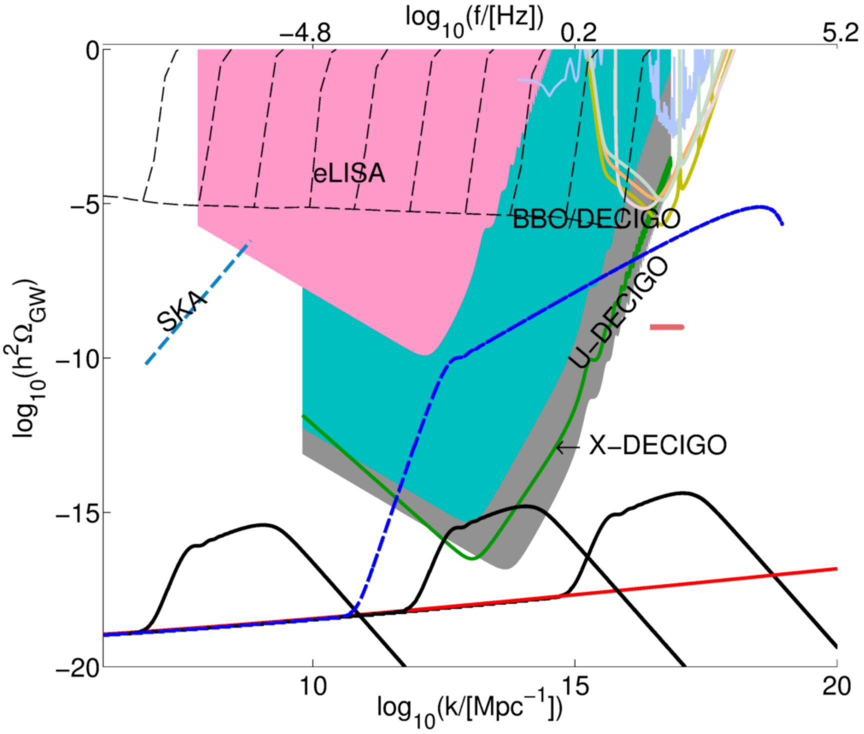

Figure 8. The spectra of induced gravitational waves for the Hilltop model $p = 2$ and $q = 4$, with $k_{max} = k_{NL}$. The black dashed lines and the cluster of solid lines in the right hand corner are defined in Fig. 5. The red line represents the induced gravitational wave spectrum for $T_r \gg 10^{10}$GeV and $N = 55$ $e-$folds. From right to left, the black solid lines correspond to the induced gravitational wave spectrum for $T_r = 10^8$GeV, $T_r = 10^5$GeV, and $T_r = 1$GeV. For illustration, we include the spectrum for a reheat temperature of $T_r = 10^5$GeV and integrated up to the maximum scale instead of the non-linear cutoff (dashed blue line).

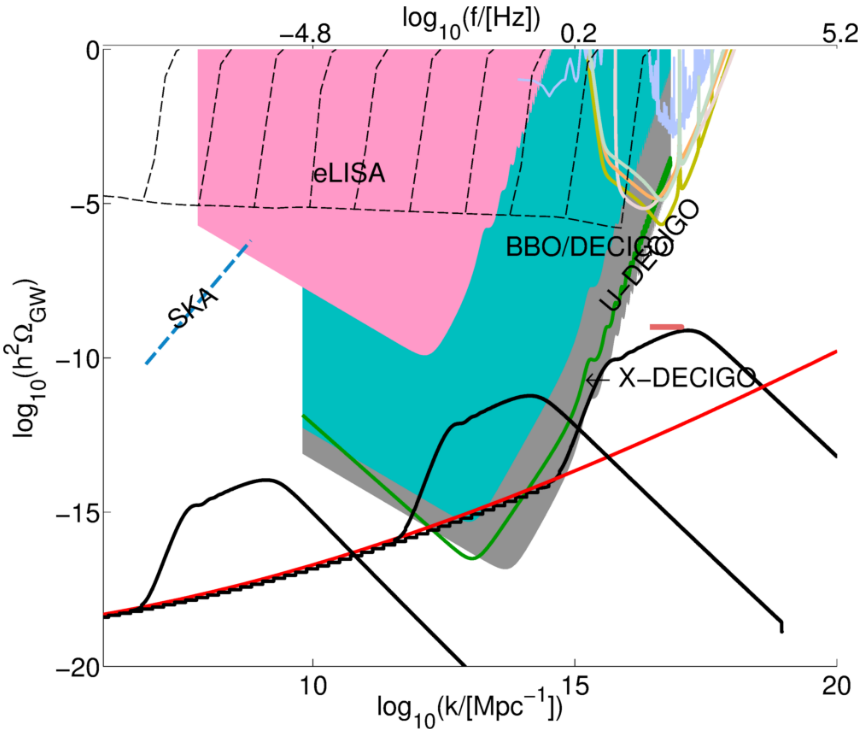

Figure 9. The spectra of induced gravitational waves for the Hilltop model $p = 2$ and $q = 2.3$, with $k_{max} = k_{NL}$. The red line represents the induced gravitational wave spectrum $T_r \gg 10^{10}$GeV and $N = 55$ $e-$folds. From right to left, the black solid lines correspond to the induced gravitational wave spectrum for $T_r = 10^8$GeV, $T_r = 10^5$GeV, and $T_r = 1$GeV. The black dashed lines and the cluster of solid lines in the right hand corner are defined in Fig. 5.

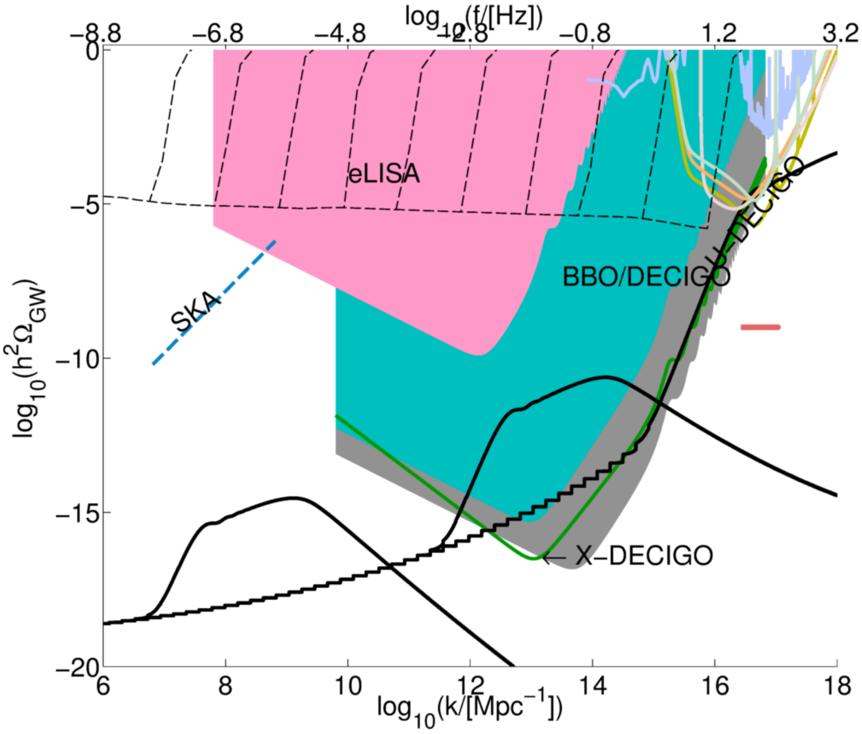

Figure 10. The spectra of induced gravitational waves for the running mass model satisfying $n_s' = 0.0039$ and $N = 57$, with $k_{max} = k_{NL}$. From right to left, the black solid lines correspond to the induced gravitational wave spectrum $T_r = 1$GeV,$T_r = 1 \times 10^5$GeV, and $T_r = 10^9$GeV. The black dashed lines and the cluster of solid lines in the right hand corner are defined in Fig. 5.

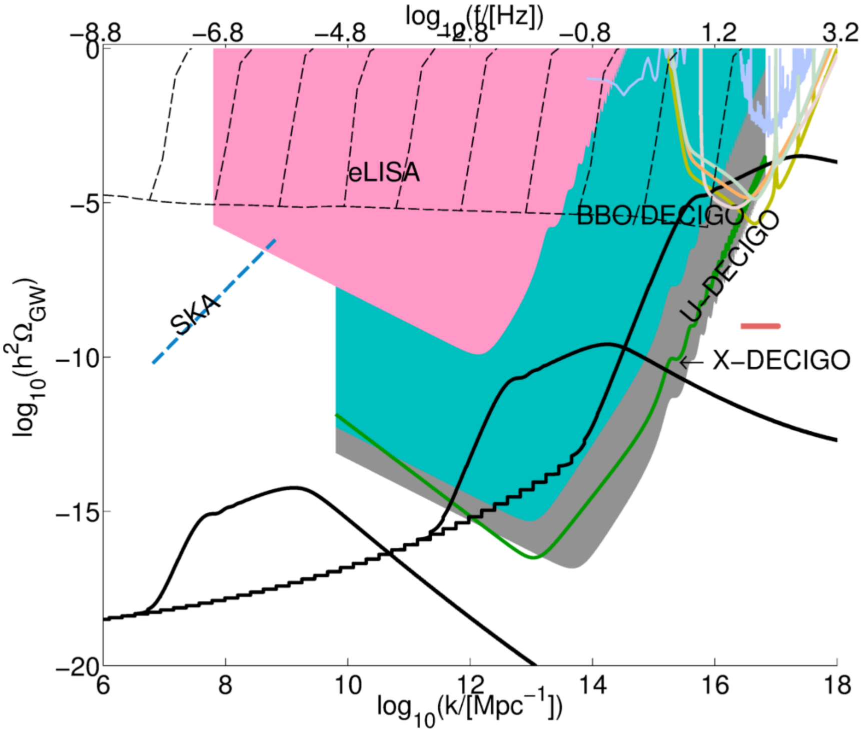

Figure 11. The spectra of induced gravitational waves for the running mass model satisfying $n_s' = 0.0043$ and $N = 57$, with $k_{max} = k_{NL}$. From right to left, the black solid lines correspond to the induced gravitational wave spectrum $T_r = 1$GeV,$T_r = 1 \times 10^5$GeV, and $T_r = 10^8$GeV.T The black dashed lines and the cluster of solid lines in the right hand corner are defined in Fig. 5.

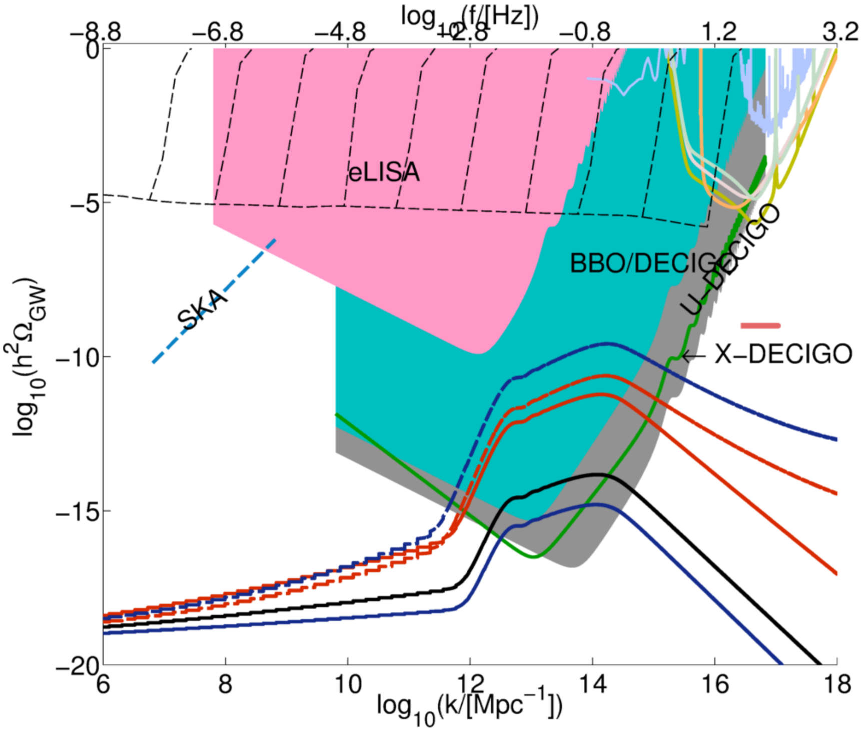

Figure 12. The spectra of induced gravitational waves for all the models plotted in the previous figures assuming a reheat temperature of $T_r = 10^5$GeV, with $k_{max} = k_{NL}$. The solid lines are hilltop with $p = 2$ $q = 2.3$ (red), $p = 2$ $q = 3$ (black) and $p = 2$ $q = 4$ (blue); the dashed lines are the running mass models with $n_s' = 0.0043$ (blue) and $n_s' = 0.0039$ (red). The black dashed lines and the cluster of solid lines in the right hand corner are defined in Fig. 5.

8 Discussion

In this work we assumed a sudden transition between early matter domination and radiation domination. In the early universe however, the Hubble time can be of the order of the decay rate of matter to radiation. In this case modes re-entering the horizon towards the end of matter domination will also experience a decaying source term and the effect shown here may be reduced, depending on how long the transition phase lasts, as is shown in Fig. 3. Therefore the results presented here are upper bounds on what the induced gravitational wave spectrum could be, with the actual spectrum possibly being only an order of magnitude or two smaller than what we calculated.

Therefore our conclusions depend on the condition that the tensor modes generated during an early matter phase survive the transition into radiation. Under this proviso, we have shown that assuming an early matter phase with $T_r = 10^5$GeV results in a spectrum of induced gravitational waves with energy densities within the range of BBO/DECIGO and cross-correlated DECIGO [69]. Since the assumption of an early matter phase truncates the PBH bound at a smaller value of k, we have shown that the running mass model generates induced gravitational waves detectable by ground based gravitational wave detectors such as LIGO, and KAGRA. This means that the RMM model with a running of $n_s' = 0.0043$ and a reheat temperature of 10^8GeV as well as the model with $n_s' = 0.0039$ and $T_r = 10^9$GeV can be ruled out since LIGO has failed to detect a gravitational signature.

Acknowledgments

We thank T.Harada, K. Koyama, S. Kuruyonagi, T. Tanaka, D. Wands, J. Yokoyama and C. Yoo for useful discussions and feedback. This work was supported in part by grant-in-aid for scientific research on innovative areas No. 24103006, No. 21111006, No. 22244030, and No. 23540327, JSPS Grant-in-Aid for Scientific Research (A) No. 21244033 and MEXT Grant-in-Aid for Scientific Research on Innovative Areas No. 24111701

A The time integral during the radiation era

$$\begin{aligned}\tilde{I}_1 = \frac{1}{4ky^3v^3}&\left\{-\cos(x)\sum_{n=1}^{4}\alpha_n\mathrm{Si}(\beta_\mathrm{n}\mathrm{x}) + \sin(\mathrm{x})\sum_{\mathrm{n=1}}^{4}(-1)^{\mathrm{n+1}}\alpha_\mathrm{n}\mathrm{ci}(\beta_\mathrm{n}\mathrm{x})\right\}\\ &+\gamma_1\sin(x) + \gamma_2\sin(vx)\sin(yx) + \gamma_3\sin(vx)\cos(yx) + \gamma_4\cos(vx)\sin(yx) + \gamma_5\cos(vx)\cos(yx)\end{aligned} \tag{A.1}$$

and the second integral is given by:

$$\begin{aligned}\tilde{I}_2 = -\frac{\alpha}{2kv^3y^3}&\left\{\cos(x)\left[-\mathrm{Si}(\beta_1\mathrm{x}) + \mathrm{Si}(\beta_2\mathrm{x}) + \mathrm{Si}(\beta_3\mathrm{x}) - \mathrm{Si}(\beta_4\mathrm{x})\right]\right.\\ &\left.+\sin(x)\left[\mathrm{ci}(\beta_1\mathrm{x}) + \mathrm{ci}(\beta_2\mathrm{x}) - \mathrm{ci}(\beta_3\mathrm{x}) - \mathrm{ci}(\beta_4\mathrm{x})\right]\right\}\\ &+\gamma_{21}\sin(x) + \gamma_{22}\sin(x(v+y)) + \gamma_{23}\sin(x(v-y)) + \gamma_{24}\cos(x(v-y)) + \gamma_{25}\cos(x(v+y))\end{aligned} \tag{A.2}$$

the coefficients in these two integrals are given in the tables below. The α_n coefficients in the first integral satisfy $\sum_{n=1}^{4}(-1)^n\alpha_n = 0$ and the α coefficient in the second integral is given by $\alpha = (v^2 - 1 + y^2)^2$.

The Si and ci terms are the sine and cosine integrals respectively [70], defined as:

$$\begin{aligned} \mathrm{Si(x)} &= \int_0^x \frac{\sin(t)}{t} dt \\ \mathrm{ci(x)} &= \int_0^x \frac{\cos(t)}{t} dt \ . \end{aligned} \tag{A.3}$$

β_1	$1 + v + y$
β_2	$-1 + v + y$
β_3	$1 + v - y$
β_4	$-1 + v - y$

Coefficient	Symbol	Expression
$\sin(x)$	γ_1	$\frac{1}{kv^2y^2}(v^2 - 3y^2 + 1)$
$\sin(vx)\sin(yx)$	γ_2	$\frac{1}{kx^3y^3v^3}(2 - x^2 - x^2y^2 + 3x^2v^2)$
$\sin(vx)\cos(yx)$	γ_3	$-\frac{2}{ky^2x^2v^3}$
$\cos(vx)\sin(yx)$	γ_4	$-\frac{2}{kx^2y^3v^2}$
$\cos(vx)\cos(yx)$	γ_5	$\frac{2}{kxy^2v^2}$
$\sin(x)$	γ_{21}	$\frac{2}{kv^2y^2}(1 - v^2 - y^2)$
$\sin(x(v - y))$	γ_{22}	$\frac{2}{kx^2v^3y^3}(v - y)$
$\sin(x(v + y))$	γ_{23}	$-\frac{2}{kx^2v^3y^3}(v + y)$
$\cos(x(v - y))$	γ_{24}	$-\frac{1}{kx^3y^3v^3}(-2 + x^2 - x^2y^2 - x^2v^2 - 2x^2vy)$
$\cos(x(v + y))$	γ_{25}	$-\frac{1}{kx^3v^3y^3}(2 - x^2 + x^2y^2 + x^2v^2 - 2x^2vy)$

Table 1. Table on the left gives the expressions for the coefficients of the arguments of the Cosine and Sine integrals in Eqs. (A.1) and (A.2). The right table gives the expressions for the τ_1 integral Eq. (A.1) (tob block) and for the τ_2 integral Eq. (A.2) (bottom block).

	1	v^4	$4v^3$	$4v^2$	$3y^4$	$4y^3$	$2y^2v^2$
α_1	$-$	$+$	$+$	$+$	$-$	$-$	$-$
α_2	$+$	$-$	$+$	$-$	$+$	$-$	$+$
α_3	$+$	$-$	$-$	$-$	$+$	$-$	$+$
α_4	$-$	$+$	$-$	$+$	$-$	$-$	$-$

Table 2. This table gives the expressions of the coefficients of the sine and cosine integrals in Eq. (A.1). Each α_n coefficient has the same parameters as the others, but the parameters differ in their respective signs. The columns to the right of the αs give the sign of the parameter defined in the column header. For example then we can read off α_1 as $-1 + v^4 + 4v^3 + 4v^2 - 3y^4 - 4y^3 - 2y^2v^2$.

References

[1] S. Matarrese, O. Pantano, and D. Saez, *General relativistic dynamics of irrotational dust: Cosmological implications*, *Phys.Rev.Lett.* **72** (1994) 320–323, [arXiv:astro-ph/9310036], [doi:10.1103/PhysRevLett.72.320].

[2] S. Matarrese, S. Mollerach, and M. Bruni, *Second order perturbations of the Einstein-de Sitter universe*, *Phys.Rev.* **D58** (1998) 043504, [arXiv:astro-ph/9707278], [doi:10.1103/PhysRevD.58.043504].

[3] S. Mollerach, D. Harari, and S. Matarrese, *CMB polarization from secondary vector and tensor modes*, *Phys.Rev.* **D69** (2004) 063002, [arXiv:astro-ph/0310711], [doi:10.1103/PhysRevD.69.063002].

[4] K. N. Ananda, C. Clarkson, and D. Wands, *The Cosmological gravitational wave background from primordial density perturbations*, *Phys.Rev.* **D75** (2007) 123518, [arXiv:gr-qc/0612013], [doi:10.1103/PhysRevD.75.123518].

[5] D. Baumann, P. J. Steinhardt, K. Takahashi, and K. Ichiki, *Gravitational Wave Spectrum Induced by Primordial Scalar Perturbations*, *Phys.Rev.* **D76** (2007) 084019, [arXiv:hep-th/0703290], [doi:10.1103/PhysRevD.76.084019].

[6] R. Saito and J. Yokoyama, *Gravitational wave background as a probe of the primordial black hole abundance*, *Phys.Rev.Lett.* **102** (2009) 161101, [arXiv:0812.4339], [doi:10.1103/PhysRevLett.102.161101, 10.1103/PhysRevLett.107.069901, 10.1103/PhysRevLett.102.161101, 10.1103/PhysRevLett.107.069901].

[7] R. Saito and J. Yokoyama, *Gravitational-Wave Constraints on the Abundance of Primordial Black Holes*, *Prog.Theor.Phys.* **123** (2010) 867–886, [arXiv:0912.5317], [doi:10.1143/PTP.123.867]. * Brief entry *.

[8] E. Bugaev and P. Klimai, *Bound on induced gravitational wave background from primordial black holes*, *JETP Lett.* **91** (2010) 1–5, [arXiv:0911.0611], [doi:10.1134/S0021364010010017]. * Brief entry *.

[9] E. Bugaev and P. Klimai, *Constraints on the induced gravitational wave background from primordial black holes*, *Phys.Rev.* **D83** (2011) 083521, [arXiv:1012.4697], [doi:10.1103/PhysRevD.83.083521].

[10] L. Alabidi, K. Kohri, M. Sasaki, and Y. Sendouda, *Observable Spectra of Induced Gravitational Waves from Inflation*, *JCAP* **1209** (2012) 017, [arXiv:1203.4663], [doi:10.1088/1475-7516/2012/09/017].

[11] K. Kohri, C.-M. Lin, and D. H. Lyth, *More hilltop inflation models*, *JCAP* **0712** (2007) 004, [arXiv:0707.3826], [doi:10.1088/1475-7516/2007/12/004].

[12] M. Drees and E. Erfani, *Running Spectral Index and Formation of Primordial Black Hole in Single Field Inflation Models*, arXiv:1110.6052.

[13] N. Seto, S. Kawamura, and T. Nakamura, *Possibility of direct measurement of the acceleration of the universe using 0.1-Hz band laser interferometer gravitational wave antenna in space*, *Phys.Rev.Lett.* **87** (2001) 221103, [arXiv:astro-ph/0108011], [doi:10.1103/PhysRevLett.87.221103].

[14] `http://tamago.mtk.nao.ac.jp/decigo/index_E.html`.

[15] H. Kudoh and A. Taruya, *Probing anisotropies of gravitational-wave backgrounds with a space-based interferometer: Geometric properties of antenna patterns and their angular power*, *Phys.Rev.* **D71** (2005) 024025, [arXiv:gr-qc/0411017], [doi:10.1103/PhysRevD.71.024025].

[16] `http://lisa.nasa.gov/`.

[17] P. Amaro-Seoane, S. Aoudia, S. Babak, P. Binetruy, E. Berti, *et al.*, *eLISA: Astrophysics and*

cosmology in the millihertz regime, arXiv:1201.3621.

[18] N. Seto and J. Yokoyama, *Probing the equation of state of the early universe with a space laser interferometer*, *J.Phys.Soc.Jap.* **72** (2003) 3082–3086, [arXiv:gr-qc/0305096], [doi:10.1143/JPSJ.72.3082].

[19] L. A. Boyle and A. Buonanno, *Relating gravitational wave constraints from primordial nucleosynthesis, pulsar timing, laser interferometers, and the CMB: Implications for the early Universe*, *Phys.Rev.* **D78** (2008) 043531, [arXiv:0708.2279], [doi:10.1103/PhysRevD.78.043531].

[20] K. Nakayama, S. Saito, Y. Suwa, and J. Yokoyama, *Space laser interferometers can determine the thermal history of the early Universe*, *Phys.Rev.* **D77** (2008) 124001, [arXiv:0802.2452], [doi:10.1103/PhysRevD.77.124001].

[21] K. Nakayama, S. Saito, Y. Suwa, and J. Yokoyama, *Probing reheating temperature of the universe with gravitational wave background*, *JCAP* **0806** (2008) 020, [arXiv:0804.1827], [doi:10.1088/1475-7516/2008/06/020].

[22] M. Joyce, *Electroweak Baryogenesis and the Expansion Rate of the Universe*, *Phys.Rev.* **D55** (1997) 1875–1878, [arXiv:hep-ph/9606223], [doi:10.1103/PhysRevD.55.1875].

[23] J. Hidalgo, L. A. Urena-Lopez, and A. R. Liddle, *Unification models with reheating via Primordial Black Holes*, *Phys.Rev.* **D85** (2012) 044055, [arXiv:1107.5669], [doi:10.1103/PhysRevD.85.044055]. Updated to match version accepted by PRD.

[24] H. Assadullahi and D. Wands, *Constraints on primordial density perturbations from induced gravitational waves*, *Phys.Rev.* **D81** (2010) 023527, [arXiv:0907.4073], [doi:10.1103/PhysRevD.81.023527].

[25] D. H. Lyth and A. R. Liddle, *The primordial density perturbation: Cosmology, inflation and the origin of structure*, .

[26] G. Hinshaw, D. Larson, E. Komatsu, D. Spergel, C. Bennett, *et al.*, *Nine-Year Wilkinson Microwave Anisotropy Probe (WMAP) Observations: Cosmological Parameter Results*, arXiv:1212.5226.

[27] C. Bennett, D. Larson, J. Weiland, N. Jarosik, G. Hinshaw, *et al.*, *Nine-Year Wilkinson Microwave Anisotropy Probe (WMAP) Observations: Final Maps and Results*, arXiv:1212.5225.

[28] A. R. Liddle and S. M. Leach, *How long before the end of inflation were observable perturbations produced?*, *Phys.Rev.* **D68** (2003) 103503, [arXiv:astro-ph/0305263], [doi:10.1103/PhysRevD.68.103503].

[29] S. Dodelson and L. Hui, *A Horizon ratio bound for inflationary fluctuations*, *Phys.Rev.Lett.* **91** (2003) 131301, [arXiv:astro-ph/0305113], [doi:10.1103/PhysRevLett.91.131301].

[30] M. Kawasaki, K. Kohri, and N. Sugiyama, *Cosmological constraints on late time entropy production*, *Phys.Rev.Lett.* **82** (1999) 4168, [arXiv:astro-ph/9811437], [doi:10.1103/PhysRevLett.82.4168].

[31] M. Kawasaki, K. Kohri, and N. Sugiyama, *MeV scale reheating temperature and thermalization of neutrino background*, *Phys.Rev.* **D62** (2000) 023506, [arXiv:astro-ph/0002127], [doi:10.1103/PhysRevD.62.023506].

[32] S. Hannestad, *What is the lowest possible reheating temperature?*, *Phys.Rev.* **D70** (2004) 043506, [arXiv:astro-ph/0403291], [doi:10.1103/PhysRevD.70.043506].

[33] K. Ichikawa, M. Kawasaki, and F. Takahashi, *The Oscillation effects on thermalization of the neutrinos in the Universe with low reheating temperature*, *Phys.Rev.* **D72** (2005) 043522, [arXiv:astro-ph/0505395], [doi:10.1103/PhysRevD.72.043522].

[34] B. Carr, K. Kohri, Y. Sendouda, and J. Yokoyama, *New cosmological constraints on primordial black holes*, *Phys.Rev.* **D81** (2010) 104019, [arXiv:0912.5297], [doi:10.1103/PhysRevD.81.104019].

[35] A. S. Josan, A. M. Green, and K. A. Malik, *Generalised constraints on the curvature perturbation from primordial black holes*, *Phys.Rev.* **D79** (2009) 103520, [arXiv:0903.3184], [doi:10.1103/PhysRevD.79.103520].

[36] J. S. Bullock and J. R. Primack, *NonGaussian fluctuations and primordial black holes from inflation*, *Phys.Rev.* **D55** (1997) 7423–7439, [arXiv:astro-ph/9611106], [doi:10.1103/PhysRevD.55.7423].

[37] P. Ivanov, *Nonlinear metric perturbations and production of primordial black holes*, *Phys.Rev.* **D57** (1998) 7145–7154, [arXiv:astro-ph/9708224], [doi:10.1103/PhysRevD.57.7145].

[38] P. Pina Avelino, *Primordial black hole constraints on non-gaussian inflation models*, *Phys.Rev.* **D72** (2005) 124004, [arXiv:astro-ph/0510052], [doi:10.1103/PhysRevD.72.124004].

[39] S. Chongchitnan and G. Efstathiou, *Accuracy of slow-roll formulae for inflationary perturbations: implications for primordial black hole formation*, *JCAP* **0701** (2007) 011, [arXiv:astro-ph/0611818], [doi:10.1088/1475-7516/2007/01/011].

[40] J. Hidalgo, *The effect of non-Gaussian curvature perturbations on the formation of primordial black holes*, arXiv:0708.3875.

[41] E. Bugaev and P. Klimai, *Formation of primordial black holes from non-Gaussian perturbations produced in a waterfall transition*, arXiv:1112.5601. v2: 11 pages, 4 figures. Several comments and references added. Version accepted by Phys. Rev. D.

[42] C. T. Byrnes, E. J. Copeland, and A. M. Green, *Primordial black holes as a tool for constraining non-Gaussianity*, *Phys.Rev.* **D86** (2012) 043512, [arXiv:1206.4188], [doi:10.1103/PhysRevD.86.043512].

[43] M. Y. Khlopov and A. Polnarev, *PRIMORDIAL BLACK HOLES AS A COSMOLOGICAL TEST OF GRAND UNIFICATION*, *Phys.Lett.* **B97** (1980) 383–387, [doi:10.1016/0370-2693(80)90624-3].

[44] M. Maggiore, *Stochastic backgrounds of gravitational waves*, arXiv:gr-qc/0008027.

[45] `http://www.ligo.caltech.edu/~jzweizig/distribution/LSC_Data/`.

[46] **KAGRA Collaboration** Collaboration, K. Somiya, *Detector configuration of KAGRA: The Japanese cryogenic gravitational-wave detector*, *Class.Quant.Grav.* **29** (2012) 124007, [arXiv:1111.7185], [doi:10.1088/0264-9381/29/12/124007].

[47] `https://dcc.ligo.org/cgi-bin/DocDB/ShowDocument?docid=2974`.

[48] **LIGO Scientific Collaboration, VIRGO Collaboration** Collaboration, B. Abbott *et al.*, *An Upper Limit on the Stochastic Gravitational-Wave Background of Cosmological Origin*, *Nature* **460** (2009) 990, [arXiv:0910.5772], [doi:10.1038/nature08278].

[49] F. A. Jenet, G. Hobbs, W. van Straten, R. Manchester, M. Bailes, *et al.*, *Upper bounds on the low-frequency stochastic gravitational wave background from pulsar timing observations: Current limits and future prospects*, *Astrophys.J.* **653** (2006) 1571–1576, [arXiv:astro-ph/0609013], [doi:10.1086/508702].

[50] G. Hobbs, D. Miller, R. Manchester, J. Dempsey, J. Chapman, *et al.*, *The Parkes Observatory Pulsar Data Archive*, arXiv:1105.5746.

[51] D. Yardley, G. Hobbs, F. Jenet, J. Verbiest, Z. Wen, *et al.*, *The Sensitivity of the Parkes Pulsar Timing Array to Individual Sources of Gravitational Waves*, arXiv:1005.1667.

[52] `http://www.atnf.csiro.au/research/pulsar/ppta/index.php?n=Main.PPTA`.

[53] K. Kohri, D. H. Lyth, and A. Melchiorri, *Black hole formation and slow-roll inflation*, *JCAP* **0804** (2008) 038, [arXiv:0711.5006], [doi:10.1088/1475-7516/2008/04/038].

[54] L. Alabidi and K. Kohri, *Generating Primordial Black Holes Via Hilltop-Type Inflation Models*,

Phys. Rev. **D80** (2009) 063511, [arXiv:0906.1398], [doi:10.1103/PhysRevD.80.063511].

[55] R. Allahverdi, A. Kusenko, and A. Mazumdar, *A-term inflation and the smallness of neutrino masses*, *JCAP* **0707** (2007) 018, [arXiv:hep-ph/0608138], [doi:10.1088/1475-7516/2007/07/018].

[56] C.-M. Lin and K. Cheung, *Super Hilltop Inflation*, *JCAP* **0903** (2009) 012, [arXiv:0812.2731], [doi:10.1088/1475-7516/2009/03/012].

[57] C.-M. Lin and K. Cheung, *Reducing the Spectral Index in Supernatural Inflation*, Phys.Rev. **D79** (2009) 083509, [arXiv:0901.3280], [doi:10.1103/PhysRevD.79.083509].

[58] I. Ben-Dayan and R. Brustein, *Cosmic Microwave Background Observables of Small Field Models of Inflation*, *JCAP* **1009** (2010) 007, [arXiv:0907.2384], [doi:10.1088/1475-7516/2010/09/007].

[59] K. Kohri and C.-M. Lin, *Hilltop Supernatural Inflation and Gravitino Problem*, *JCAP* **1011** (2010) 010, [arXiv:1008.3200], [doi:10.1088/1475-7516/2010/11/010].

[60] S. Hotchkiss, A. Mazumdar, and S. Nadathur, *Observable gravitational waves from inflation with small field excursions*, arXiv:1110.5389.

[61] E. D. Stewart, *Flattening the inflaton's potential with quantum corrections*, Phys.Lett. **B391** (1997) 34–38, [arXiv:hep-ph/9606241], [doi:10.1016/S0370-2693(96)01458-X].

[62] L. Covi, D. H. Lyth, and L. Roszkowski, *Observational constraints on an inflation model with a running mass*, *Phys. Rev.* **D60** (1999) 023509, [arXiv:hep-ph/9809310], [doi:10.1103/PhysRevD.60.023509].

[63] L. Covi and D. H. Lyth, *Running-mass models of inflation, and their observational constraints*, *Phys. Rev.* **D59** (1999) 063515, [arXiv:hep-ph/9809562], [doi:10.1103/PhysRevD.59.063515].

[64] D. H. Lyth and L. Covi, *Observational constraints on the spectral index of the cosmological curvature perturbation*, *Phys. Rev.* **D62** (2000) 103504, [arXiv:astro-ph/0002397], [doi:10.1103/PhysRevD.62.103504].

[65] S. M. Leach, I. J. Grivell, and A. R. Liddle, *Black hole constraints on the running mass inflation model*, *Phys. Rev.* **D62** (2000) 043516, [arXiv:astro-ph/0004296], [doi:10.1103/PhysRevD.62.043516].

[66] L. Covi and D. H. Lyth, *Global fits for the spectral index of the cosmological curvature perturbation*, *Mon. Not. Roy. Astron. Soc.* **326** (2001) 885, [arXiv:astro-ph/0008165], [doi:10.1046/j.1365-8711.2001.04466.x].

[67] L. Covi, D. H. Lyth, and A. Melchiorri, *New constraints on the running-mass inflation model*, *Phys. Rev.* **D67** (2003) 043507, [arXiv:hep-ph/0210395], [doi:10.1103/PhysRevD.67.043507].

[68] L. Covi, D. H. Lyth, A. Melchiorri, and C. J. Odman, *The running-mass inflation model and WMAP*, *Phys. Rev.* **D70** (2004) 123521, [arXiv:astro-ph/0408129], [doi:10.1103/PhysRevD.70.123521].

[69] H. Kudoh, A. Taruya, T. Hiramatsu, and Y. Himemoto, *Detecting a gravitational-wave background with next-generation space interferometers*, Phys.Rev. **D73** (2006) 064006, [arXiv:gr-qc/0511145], [doi:10.1103/PhysRevD.73.064006].

[70] M. Abramowitz and I. A. Stegun, *Handbook of Mathematical Functions with Formulas, Graphs, and Mathematical Tables.* Dover, New York, ninth dover printing, tenth gpo printing ed., 1964.